

Primordial black hole formation by vacuum bubbles II

Heling Deng*

Physics Department, Arizona State University, Tempe, AZ 85287, USA

Abstract

The discoveries of LIGO/Virgo black holes in recent years have revitalized the study of primordial black holes. In this work we investigate a mechanism where primordial black holes are formed by vacuum bubbles that randomly nucleate during inflation through quantum tunneling. After inflation, these bubbles typically run into the ambient radiation fluid with a large Lorentz factor. In our previous work, we assumed the bubble fields are strongly coupled to the standard model particles so that the bubble wall is impermeable. Here we complete this picture by considering bubbles interacting with the fluid only through gravity. By studying the scenario in several limits, we found that black holes could form in the either subcritical or supercritical regime. Depending on the model parameters, the resulting mass spectrum of the black holes could be wide or narrow, and may develop two peaks separated by a large mass range. With different spectra, these black holes may account for the LIGO/Virgo black holes, supermassive black holes, and may play an important role in dark matter.

*Electronic address: dengheling@gmail.com

I. INTRODUCTION

Primordial black holes (PBHs) are hypothetical black holes formed in the early universe, usually during the radiation dominated era. In principle, a PBH could have a mass ranging from the Planck mass ($M_{\text{Pl}} \sim 10^{-5}$ g) to many orders of magnitude larger than the solar mass ($M_{\odot} \sim 10^{33}$ g). Due to Hawking radiation, PBHs formed with masses below $\sim 10^{15}$ g would have evaporated by now, hence many efforts to constrain them have been focused on nonevaporating ones with $M \gtrsim 10^{15}$ g.

Recent interest in PBHs is to a great extent stimulated by the discoveries in LIGO/Virgo: gravitational waves were detected from merging black holes of masses $\mathcal{O}(10\text{--}100)M_{\odot}$ [1]. These black holes are slightly heavier than what would be expected for ordinary stellar black holes, and one intriguing hypothesis is that they have a primordial origin [2–4].

LIGO/Virgo events also revitalized the study on PBH dark matter (see ref. [5] for a recent review). At the moment, there are stringent constraints on the fraction of dark matter in PBHs within the mass range $10^{15}\text{--}10^{47}$ g from the observed dynamical, microlensing and astrophysical effects (see refs. [6, 7] and references therein). Some up-to-date upper bounds $f_{\text{max}}(M)$ for a monochromatic mass spectrum are shown in fig. 1 (adapted from fig. 10 in ref. [7]), with colored regions ruled out by observations. The possibility that PBHs account for all dark matter has been excluded for most black hole masses. In fact, LIGO/Virgo is among the observations to recently close one of the windows: if PBHs play any role in dark matter, they can only constitute a small fraction at around $10M_{\odot}$, otherwise the black hole merger rate inferred by LIGO/Virgo should have been larger [8]. Another tight bound imposed recently is from the study of the CMB anisotropy in ref. [9], which considers the effect of disk and spherical accretion of a halo around PBHs, and strongly constrains the population of PBHs in the mass range around $1\text{--}10^4 M_{\odot}$, reaching $f_{\text{max}}(10^4 M_{\odot}) < 3 \times 10^{-9}$. We can see from fig. 1 that the only window allowing PBHs to constitute all dark matter is $\sim 10^{17}\text{--}10^{23}$ g.

Another motivation to the study of PBHs is to explain supermassive black holes (SMBHs) at the center of most galaxies [10, 11]. These black holes have masses ranging from around $10^6 M_{\odot}$ to $10^{10} M_{\odot}$, which cannot be explained by standard accretion models [12], and observations of quasars indicate that many of them were already in place at high redshifts (see ref. [13] for a review). One is then led to speculate that SMBHs were seeded by PBHs,

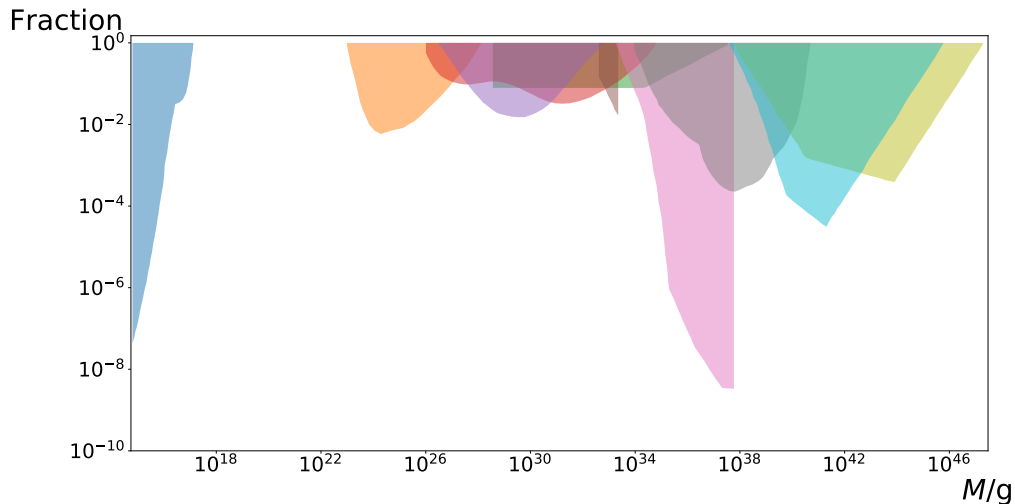


FIG. 1: Some conservative constraints on the fraction of dark matter in PBHs for a monochromatic mass spectrum (see ref. [7] and references therein). Colored regions have been excluded by observations including (from left to right) evaporation (blue), HSC (orange), EROS (red), OGLE (purple), Icarus (green), LIGO/Virgo (brown), Planck (pink), X-ray binaries (gray), halo dynamical friction (cyan), and large scale structure (olive).

which could have large masses by birth [14–18]. It was shown in ref. [9, 16] that primordial seeds as massive as $\sim 10^3 M_\odot$ can attain sufficient accretion and grow to SMBHs.

PBHs can be formed in a variety of mechanisms. The most popular and natural scenario is PBH formation from inflationary density perturbations [19–24]: after inflation, a large overdensity of superhorizon scale can overcome pressure and collapse into a black hole at Hubble reentry. However, provided the primordial perturbations are Gaussian, the formation of these black holes with masses $\sim 10^5\text{--}10^9 M_\odot$ has been ruled out in any appreciable numbers due to the strong bounds on μ -distortions in CMB [25–28]. In order to account for the seeds of SMBHs, one thus needs an inflationary model that happens to give a relatively large density of PBHs with $M \sim 10^3 M_\odot$ and a negligible density at $M \sim 10^5 M_\odot$. Other ways to circumvent this problem include considering perturbations with a highly non-Gaussian tail (e.g., [29]), and other PBH mechanisms unrelated to density perturbations from quantum fluctuations (e.g., collapse of cosmic strings [30–33], bubble collisions [34–36], and collapse of closed domain walls [32, 37, 38]).

In this paper we shall turn to the last approach and investigate a simple and natural

mechanism, where the black holes are formed by vacuum bubbles that nucleate through quantum tunneling during inflation. Similar models were constructed and analyzed in ref. [39], and studied in detail by numerical work in refs. [40, 41], where we focused on two specific scenarios: (1) permeable spherical domain walls immersed in the radiation dominated universe, and (2) vacuum bubbles with impermeable walls that completely reflect the radiation fluid after inflation. Black holes could be formed in either case with a distinctive and extended mass distribution. In the second scenario, we assumed strong couplings between the fields in the standard model and those producing the bubble. As such, standard model particles could acquire large masses in the bubble interior, and particles outside bounce back when they hit the walls. Bubbles running into the ambient fluid with a large Lorentz factor would then lose much of their energy due to momentum transfer. This takes place almost instantaneously compared to the Hubble time, and the bubbles do not grow much relative to the Hubble flow before turning into black holes. In this work, we will complete this picture and consider vacuum bubbles interacting with the FRW fluid only through gravitation. The bubbles could then grow to much larger sizes as the fluid freely flows in. We found that this would lead to a drastic change in the mass spectrum of the resulting black holes, especially on the end of the small ones. Depending on the model parameters, the spectrum could be either wide or narrow, and could be consistent with all the current constraints, while in the meantime being able to play the role of dark matter, LIGO/Virgo black holes and/or SMBHs. Our main result are shown in fig. 5.

The rest of the paper is organized as follows. The behavior of bubble expansion after inflation will be discussed in section II, followed by the discussion of black hole formation in some particular situations in section III. In section IV we will compute the corresponding mass spectrum of the resulting black holes, and section V will show how the spectrum is constrained by current observations. Conclusions are summarized and discussed in section VI. We set $c = \hbar = G = 1$, and the Planck mass $M_{Pl} = \sqrt{\hbar c/G}$ throughout the paper.

II. BUBBLE EXPANSION

Inflation is usually described by the evolution of a scalar field called the inflaton. The inflaton slowly rolls down its potential at a large energy scale that remains almost a constant, which drives a nearly exponential expansion. After the universe grows by over 30 orders

of magnitude, the inflaton eventually rolls down to a valley corresponding to our current vacuum. In general, the inflaton may run in a multi-dimensional potential, including a number of other vacua separated by barriers. Due to the effect of quantum tunneling, a bubble may nucleate, with the inflaton in a small, spherical region transiting to a new vacuum, where the energy scale is smaller than the inflationary scale, while the exterior region continues its quasi-de Sitter expansion.

Let ρ_i be the inflationary density, ρ_b the interior vacuum density and σ the surface tension (or surface energy density) of the bubble wall, with $\rho_i > \rho_b$. We define $H_i \equiv (8\pi\rho_i/3)^{1/2}$, $H_b \equiv (8\pi\rho_b/3)^{1/2}$ and $H_\sigma \equiv 2\pi\sigma$. On dimensional grounds, $H_i \sim \eta_i^2/M_{Pl}$, $H_b \sim \eta_b^2/M_{Pl}$ and $H_\sigma \sim \eta_\sigma^3/M_{Pl}^2$, where η_i , η_b and η_σ are the energy scales of the corresponding quantities. After nucleation, the bubble expands due to pressure difference between two sides of the wall, with a Lorentz factor approaching [42]

$$\gamma_i = \frac{[(\rho_i + \rho_b + 6\pi\sigma^2)^2 - 4\rho_i\rho_b]^{1/2}}{3\sigma H_i}. \quad (1)$$

If η_i dominates over η_b and η_σ , this reduces to

$$\gamma_i \approx \frac{\rho_i}{3\sigma H_i} \sim \frac{\eta_i^2 M_{Pl}}{\eta_\sigma^3} \gg 1. \quad (2)$$

Therefore, a typical bubble would expand with a large Lorentz factor at the end of inflation. As the inflaton rolls from the quasi-de Sitter vacuum to ours, the shape of the barrier between the bubble interior and the slow-roll path changes, which may cause a significant change in the bubble wall tension. In the following we regard the wall tension after inflation as a free parameter, and will continue calling it σ . Hence the free parameters of the bubble are H_i, H_b, H_σ and γ_i (later we will also include the bubble nucleation rate).

Let t_i be the time when inflation ends. After t_i , the exterior vacuum thermalizes into hot radiation, and the bubble wall runs into the ambient radiation fluid with a large γ_i . We assume the thermalization occurs instantaneously so that the radiation density at t_i is $\rho_i = 3/32\pi t_i^2$. If there is no interaction between the bubble and the fluid other than gravity, the fluid freely penetrates the wall, and the exterior spacetime can be described by a flat FRW metric,

$$ds^2 = dt^2 - a^2(t)(dr^2 + r^2 d\Omega^2), \quad (3)$$

where $a(t) \equiv (t/t_i)^{1/2}$. Since both the interior vacuum pressure and the wall tension point inwards, the bubble would slow down and come to a halt with respect to the Hubble flow

at some time denoted by t_s . If γ_i is large and ρ_b and σ small, the bubble would grow significantly. To be more specific, let $a_s \equiv a(t_s) = (t_s/t_i)^{1/2}$, we are mainly interested in the cases where $a_s \gg 1$. If $a_s \sim 1$, the bubble does not grow much relative to the Hubble flow before turning around, and negligible amount of radiation flows into the bubble. As the bubble shrinks, an empty layer would be formed between the bubble wall and the radiation fluid. This would then be similar to the scenario discussed in ref. [41], where the fluid is assumed to be completely reflected by the bubble wall and the bubble stops expanding with the fluid almost immediately after t_i . We will see that assuming $a_s \gg 1$ would lead to different features in the mass spectrum of the resulting black holes.

Let $\chi(t)$ be the comoving radius of the bubble wall for an exterior FRW observer. The bubble runs into the radiation at a speed close to the speed of light, so the trajectory of the wall can be approximated by $a\dot{\chi} \approx 1$ (at least at early times), where the overdot represents the first derivative with respect to t . This gives

$$\chi(t) \approx \chi_i + 2\sqrt{t_i}(\sqrt{t} - \sqrt{t_i}), \quad (4)$$

where $\chi_i \equiv \chi(t_i)$. Hence the comoving radius of the bubble wall at t_s is approximately

$$\chi_s \equiv \chi(t_s) \sim \chi_i + a_s H_i^{-1}, \quad (5)$$

and the physical radius is

$$R_s \equiv a(t_s)\chi_s \sim a_s \chi_i + a_s^2 H_i^{-1}. \quad (6)$$

The equation of motion of the wall can be more precisely determined by matching the spacetimes inside and outside the bubble (see appendix),

$$\ddot{\chi} + (4 - 3a^2\dot{\chi}^2) H\dot{\chi} + \frac{2}{a^2\chi} (1 - a^2\dot{\chi}^2) = - \left(\frac{\rho_b}{\sigma} + 6\pi\sigma \right) \frac{(1 - a^2\dot{\chi}^2)^{3/2}}{a}, \quad (7)$$

where $H \equiv \dot{a}/a = (2t)^{-1}$ is the Hubble parameter in the exterior region. In principle, this equation is valid only before the peculiar expansion speed of the wall $a\dot{\chi}$ decreases to the speed of sound (corresponding to a Lorentz factor $\gamma = \sqrt{3/2}$), because after this time information inside the bubble could affect the exterior spacetime. However, if the wall tension σ is sufficiently small, as assumed through out the paper, fluid nearby is barely perturbed by the wall's repulsion when the bubble expands. In addition, we shall be interested in the following two limits: small ρ_b and large ρ_b . If the interior vacuum density ρ_b is much smaller

than the radiation density during bubble expansion, radiation inside the bubble barely gets diluted by the vacuum energy, so that the wall basically lives in a homogeneous background when expanding. If ρ_b is sufficiently large, i.e., the vacuum pressure dragging the bubble is sufficiently large, the bubble would first expand almost at the speed of light for a while, then turns around and acquires a large speed within a very short time. In either limit, we expect eq. (7) to give a good approximation of how the Lorentz factor of the wall decreases from γ_i to 1.

For a bubble far beyond the Hubble horizon at t_i , eq. (7) has an analytic solution. It is shown in the appendix that, if χ_i is sufficiently large ($\chi_i \gg H_i^{-1}$), the third term on the left hand side can be neglected, and a_s becomes a constant independent of χ_i (eq. (49)),

$$a_s = \left[\frac{5\gamma_i}{2t_i} \left(\frac{\rho_b}{\sigma} + 6\pi\sigma \right)^{-1} + 1 \right]^{1/5}. \quad (8)$$

In the case that the bubble wall tension σ does not change significantly after inflation, this, along with eq. (2), gives

$$a_s \sim \left(\frac{H_i^2}{H_b^2 + H_\sigma^2} \right)^{1/5}, \quad (9)$$

which is much larger than 1 if $H_i \gg H_b, H_\sigma$. Since the third term on the left hand side of eq. (7) tends to slow down the bubble wall, the actual a_s could be significantly smaller. For more general cases, we need to numerically solve eq. (7) in order to find out the bubble wall's trajectory before t_s . With the bubble size at t_s , we will be able to find an estimate for the mass of the black hole formed by the bubble.

III. BLACK HOLE FORMATION

After t_s , the bubble turns around for an exterior FRW observer and interacts with the interior inhomogeneous fluid, which has been influenced by the bubble wall and the interior vacuum as the wall passes through. In order to fully understand what will happen to the bubble, one may need to turn to numerical study, which shall not be pursued here. In the following we will investigate three limits, where the fate of the bubble can easily be predicted, and we believe they together provide a more or less complete picture of black hole formation in our model. We found that the resulting black holes in the first limit have a mass spectrum with the most interesting features, so we shall mainly focus on this limit

from the next section. The reader may thus skip the discussion of the second and the third limits (subsections III B and III C) for the main results in this work.

A. Negligible ρ_b ($\rho_b \approx 0$)

For the first limit, we assume the interior vacuum density ρ_b to be so small that the vacuum's gravitational effect is completely negligible. As the bubble expands into the homogeneous radiation, the ambient fluid flows into the interior vacuum, which is now essentially Minkowski. Part of the fluid forms a spherical shock wave that propagates inwards at the speed of sound, which then implodes at the bubble center. It is possible that, due to the massive accretion at the center, a black hole would form during the implosion. If there is not enough fluid to form a black hole, the wave would get reflected and damped as it propagates outwards as an overdense wave. Both phenomena are interesting on their own, but we do not intend to investigate them here, since the implosion is not expected to affect the evolution of the bubble, which takes place far from the central region. On the other hand, part of the fluid inside the bubble, instead of going to the center, propagates outwards (following the bubble wall) as a rarefaction wave, also at the speed of sound. These processes are schematically shown in fig. 2.

Since the interior vacuum is negligible, the bubble can be treated as a spherical domain wall moving in the background of homogeneous radiation, much like the case we considered in ref. [40], where the domain wall is comoving with the expanding universe after inflation, and behaves like a test wall. The main difference here is that the wall comes to a stop with respect to the Hubble flow at t_s instead of t_i .

After t_s , the comoving radius of the bubble begins to decrease. A small bubble would later reenter the Hubble horizon, shrink due to the wall tension, and eventually collapse into a black hole. This is what we call the “subcritical” regime. The resulting black hole mass is estimated to be the energy on the bubble wall when the bubble reaches its maximum physical size: $M \sim 4\pi\sigma R_{max}^2$ [40].

Furthermore, if the background radiation is homogeneous before the bubble size reaches R_{max} , since the bubble collapses soon after Hubble crossing, R_{max} can be approximated by the Hubble horizon R_H a test wall would fall within (in an undisturbed FRW universe). We have $R_H = a(t_H)\chi_s = (t_H/t_i)^{1/2}\chi_s$, where $t_H = R_H/2$ is the time at Hubble crossing. This

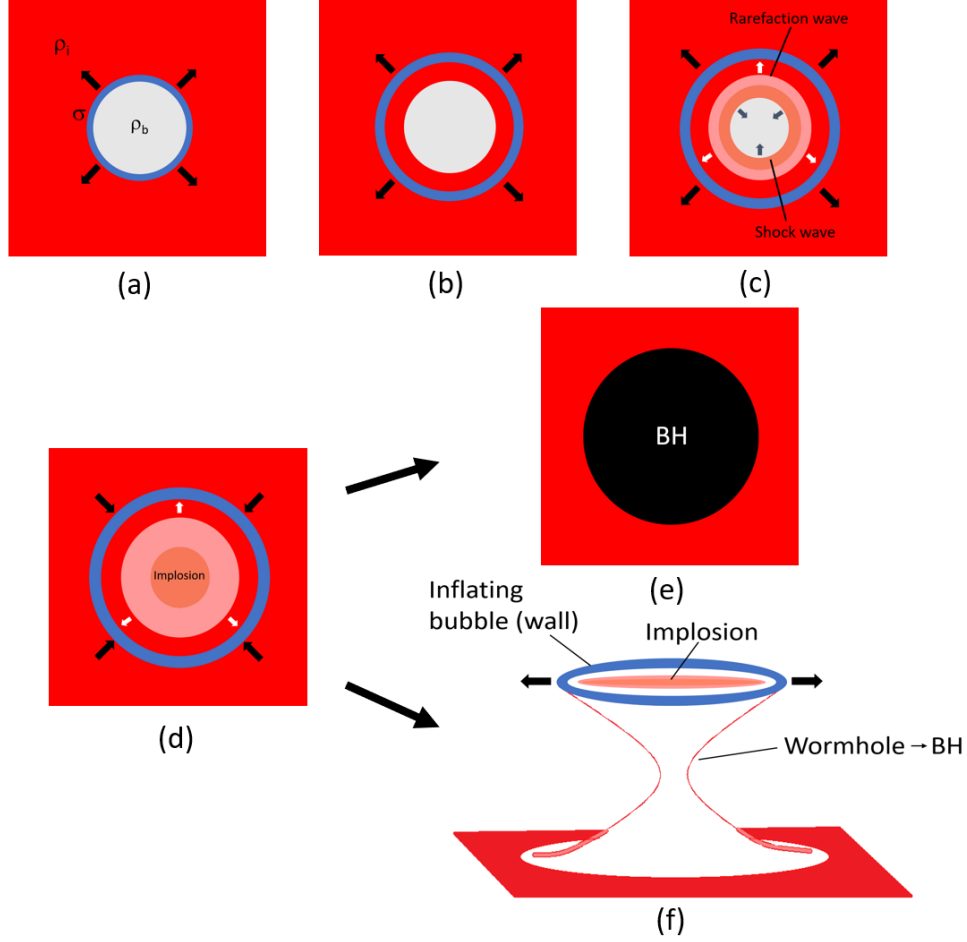


FIG. 2: Cartoon pictures illustrating bubble evolution and black hole formation in the limit of negligible ρ_b . (a) At the end of inflation, the exterior inflatons turn into radiation fluid with density ρ_i . The bubble runs into the fluid with a large Lorentz factor. (b) fluid freely flows inside as the bubble expands into the homogeneous background. (c) Part of the fluid inside the bubble forms a shock wave propagating inwards; part of the fluid forms a rarefaction wave that propagates outwards, following the expanding bubble. (d) The shock wave implodes at the bubble center, which may turn into a black hole or a reflected overdense wave. For an exterior observer, the bubble begins to turn around at t_s . (e) The bubble shrinks and collapses into a black hole (subcritical), regardless what happens inside the bubble. (f) If $H_\sigma^{-1} \ll H^{-1}$, the bubble wall would inflate and grow into a baby universe. This creates a wormhole outside the bubble. The wormhole would eventually close up and turn into a black hole (supercritical). The white regions inside and “outside” the bubble represent two almost empty shells produced by the repulsive domain wall. For an exterior FRW observer, there is a spherical rarefaction wave propagating outwards.

then gives $R_{max} \sim R_H = H_i \chi_s^2$.

However, this result is only valid if R_{max} (or R_H) is reached before the rarefaction wave inside the bubble catches up with the bubble (see fig. 2(d)(e)). The wave moves at the speed of sound, which is more than half of the expansion speed of the Hubble horizon, so it is possible that the bubble and the rarefaction wave meet before t_H . To be more specific, let $\chi_w(t)$ be the comoving radius of the rarefaction wave front, which satisfies $a\dot{\chi}_w = c_s$ (where $c_s = 1/\sqrt{3}$ is the speed of sound) with initial condition $\chi_w(t_i) = \chi_i$. Then we have

$$\chi_w(t) = \chi_i + 2c_s\sqrt{t_i} \left(\sqrt{t} - \sqrt{t_i} \right). \quad (10)$$

When it catches up with the test wall at t , we have $\chi_w(t) = \chi_s$, which gives $t \sim H_i (\chi_s - \chi_i)^2$. This would be smaller than $t_H \sim H_i \chi_s^2$ if $\chi_s \sim \chi_i$, in which case the bubble's comoving radius at t_i is so large that it does not grow much before t_s . Therefore, in order to use the result $R_{max} \sim R_H$, we need $\chi_s - \chi_i \sim a_s H_i^{-1}$ to be at least comparable to χ_i for all subcritical bubbles. In the following we assume this condition is satisfied, and leave more discussion to section VI. Therefore, the mass of the black hole from subcritical bubbles is estimated to be $M \sim 4\pi\sigma R_H^2 \sim H_\sigma H_i^2 \chi_s^4$.

On the other hand, it is known that a planar domain wall tends to inflate on the wall surface with a constant rate H_σ [43, 44]. If the time scale H_σ^{-1} is much smaller than $2t_s$ (the Hubble time at t_s), which means the time it takes for the bubble size to double is much shorter than the time it takes for the size of the universe to double, the bubble would inflate. A wormhole would be created outside as the inflating bubble is surrounded by non-inflating radiation. The bubble grows without bound in a baby universe, which is connected to us by the wormhole throat. The wormhole throat would eventually pinch off, turning into a black hole (fig. 2(f)). This is what we call the “supercritical” regime. Due to the repulsive nature of the domain wall, the wall would be sandwiched by two almost empty layers (white regions in fig. 2(f)). For an FRW observer, the bubble wall turns around after t_s and some fluid with lower density flows out. What is left in the exterior universe is a rarefaction wave propagating outwards into the homogeneous fluid at the speed of sound¹. It is suggested by the simulations in ref. [40] that the black hole mass would be comparable to the horizon mass surrounded by the wave front of the rarefaction wave at its Hubble crossing. Let the

¹ Note that this is not the rarefaction wave inside the bubble.

comoving radius of the wave front be $\chi_w(t)$, which satisfies $a\dot{\chi}_w = c_s$ with initial condition $\chi_w(t_s) = \chi_s$. The solution is

$$\chi_w(t) = \chi_s + 2c_s\sqrt{t_i} \left(\sqrt{t} - \sqrt{t_s} \right). \quad (11)$$

At Hubble crossing, we have $a(t)\chi_w(t) = 2t$, which gives the horizon mass

$$M \sim H_i \left(\chi_s - c_s a_s H_i^{-1} \right)^2. \quad (12)$$

This is the estimate of the black hole mass for supercritical bubbles. Note that the value of a_s for a certain χ_i is determined by solving eq. (7).

In conclusion, we can roughly approximate the black hole masses in the limit of negligible ρ_b by²

$$M \sim \begin{cases} H_\sigma H_i^2 \chi_s^4, & M_{min} < M < M_* \\ H_i \left(\chi_s - c_s a_s H_i^{-1} \right)^2, & M > M_* \end{cases}, \quad (13)$$

where the minimum mass M_{min} is from the fact that only bubbles with $\chi_i > H_i^{-1}$ would collapse into black holes; smaller ones are inside the Hubble horizon as they grow, and would eventually shrink and disappear. The transition mass M_* in eq. (13) characterizes the scale that connects the subcritical and supercritical regimes. Note that $\chi_s - c_s a_s H_i^{-1} \sim \chi_i + (1 - c_s) a_s H_i^{-1} \sim \chi_s$, so the supercritical black hole mass is approximately $M \sim H_i \chi_s^2$. Then the transition mass can be given by

$$M_* \sim H_\sigma^{-1}, \quad (14)$$

which corresponds to a bubble with radius

$$\chi_* \sim \left(\frac{H_i}{H_\sigma} \right)^{1/2} H_i^{-1} \quad (15)$$

at t_s . For such a critical bubble, the radiation density at Hubble crossing is $\rho_r(t_H) = \rho_i(t_i/t_H)^2 \sim \rho_i(t_i/\chi_*)^4 \sim H_\sigma^2$, which is much larger than ρ_b if $H_\sigma \gg H_b$. Hence the gravitational effect of the interior vacuum can indeed be neglected, and subcritical bubbles can be regarded as domain walls living in an FRW background before entering the horizon.

² Strictly speaking, there should be a prefactor $\sim \mathcal{O}(1-10)$ in eq. (13) from omitted prefactors in the mass estimates, as well as from mass accretion after black hole formation, but this does not affect our results by much.

Moreover, when a subcritical bubble forms a black hole, the contribution from the interior vacuum to the mass is $\sim H_b^2 M^3 < (H_b M_*)^2 M \sim (H_b/H_\sigma)^2 M \ll M$ if $H_b \ll H_\sigma$. This means the black hole mass mainly comes from the (kinetic) energy of the bubble wall, which is consistent with the subcritical scenario discussed before.

B. Small ρ_b ($\rho_b \ll \rho_r(t_s)$)

For the second limit, we shall consider a ρ_b much smaller than the exterior radiation density ρ_r when the bubble comes to a stop with respect to the Hubble fluid, i.e., $\rho_b \ll \rho_r(t_s)$. This is the case when, for instance, the bubble wall tension σ does not change much after inflation: by eq. (9), we have $\rho_b \lesssim \rho_i a_s^{-5}$; on the other hand, due to Hubble expansion, we have $\rho_i = \rho_r(t_s) a_s^4$; hence $\rho_b \lesssim \rho_i a_s^{-5} = \rho_r(t_s) a_s^{-1} \ll \rho_r(t_s)$ (the last step is from our assumption that $a_s \gg 1$). This implies the interior spacetime near the bubble wall can still be approximated by an FRW universe dominated by radiation before t_s . After t_s , the bubble's comoving radius begins to decrease but its physical size continues to grow. During this course, the radiation density inside the bubble decreases and may become comparable to ρ_b , then the bubble interior (near the wall) is dominated by radiation and a vacuum energy.

A small bubble, after reaching its maximum size, would shrink and collapse into a black hole. We expect the black hole mass to be comparable to the mass of the bubble (interior vacuum energy plus bubble wall energy) when the bubble size reaches the maximum R_{max} . After t_s , the bubble wall's trajectory is governed by (eq. (52))

$$\ddot{\chi} + (4 - 3a^2\dot{\chi}^2) H\dot{\chi} + \frac{2}{a^2\chi} (1 - a^2\dot{\chi}^2) = - \left(\frac{\rho_b}{\sigma} - 6\pi\sigma \right) \frac{(1 - a^2\dot{\chi}^2)^{3/2}}{a}. \quad (16)$$

Here the scale factor and the Hubble parameter are solutions of the following Friedmann equations:

$$H^2 = \frac{8\pi}{3} (\rho_b + \rho_r^{(in)}), \quad (17)$$

$$\frac{\ddot{a}}{a} = \frac{8\pi}{3} (\rho_b - \rho_r^{(in)}). \quad (18)$$

where $\rho_r^{(in)}(t)$ is the interior radiation density near the bubble wall. The initial conditions are $a(t_s) = a_s$ and $H(t_s) \approx 1/2t_s$. Then we can solve eq. (16) with initial conditions $\chi(t_s) = \chi_s$

and $\dot{\chi}(t_s) \approx 0$. Then the mass of the black hole from bubble collapse is estimated to be

$$M \sim \frac{4}{3}\pi\rho_b R_{max}^3 + 4\pi\sigma R_{max}^2 - 8\pi\sigma^2 R_{max}^3, \quad (19)$$

independent of radiation. Here the first term is the interior vacuum energy, the second is the bubble wall's surface energy, and the third is the wall's binding energy. It is shown in the appendix that there is a more precise way to find M , but the above equation gives a good estimate.

If during the course of bubble growth ρ_b becomes comparable to $\rho_r^{(in)}$ and the bubble size exceeds $\sim H_b^{-1}$, the bubble would inflate. Similar to the supercritical scenario discussed in the last subsection, the inflating bubble grows in a baby universe connected to our universe by a wormhole, which would later close off and turn into a black hole. Ref. [41] suggests that the mass of the black hole from such a bubble can also be estimated to be $M \sim H_i (\chi_s - c_s a_s H_i^{-1})^2$, the same as that from the last subsection.

C. Large ρ_b ($\rho_b \gtrsim \rho_r(t_s)$)

The exterior radiation density is initially larger than the interior vacuum density ($\rho_i > \rho_b$), but it gets diluted by the cosmic expansion as the bubble grows. For the third limit, we assume ρ_b to be sufficiently large so that it is comparable to or much larger than the exterior radiation density $\rho_r(t)$ at t_s , i.e., $\rho_b \gtrsim \rho_r(t_s)$. By the definition of a_s , we have

$$\rho_i a_s^{-4} = \rho_r(t_s) \lesssim \rho_b. \quad (20)$$

Then the bubble radius at t_s satisfies (eq. (6))

$$R_s \sim a_s \chi_i + a_s^2 H_i^{-1} > a_s^2 H_i^{-1} = \left(\frac{8\pi}{3} \rho_i a_s^{-4} \right)^{-1/2} \gtrsim \left(\frac{8\pi}{3} \rho_b \right)^{-1/2} = H_b^{-1}. \quad (21)$$

Note that H_b^{-1} is the de Sitter horizon associated with the interior vacuum. Since $\rho_b \gtrsim \rho_r(t_s)$, $R_s \gtrsim H_b^{-1}$ implies all bubbles would inflate in this limit (fig. 3), and the resulting black hole masses are given by $M \sim H_i (\chi_s - c_s a_s H_i^{-1})^2$.

IV. MASS SPECTRUM

In the previous sections we have shown how a black hole could be formed by a vacuum bubble and estimated the black hole mass as a function of the bubble radius at t_s in three

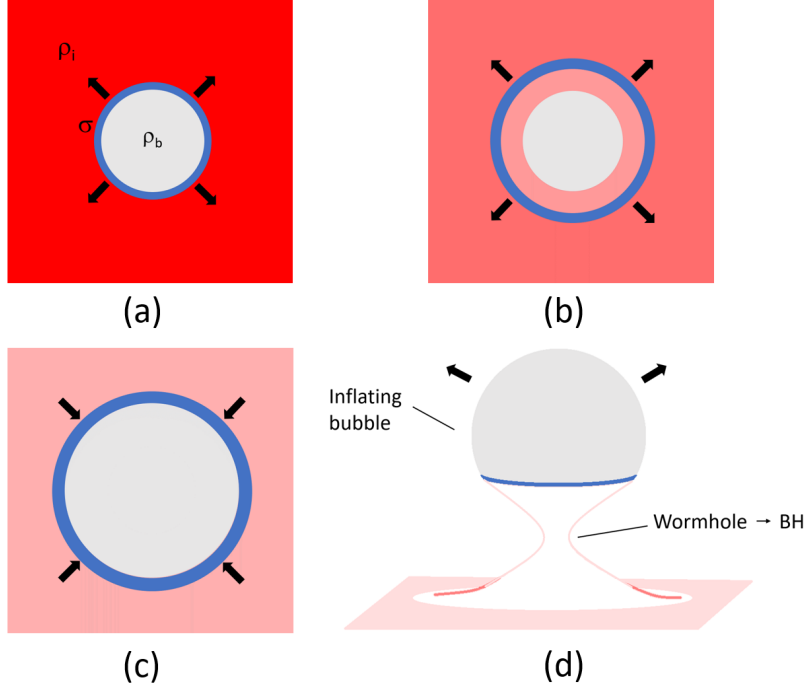


FIG. 3: Cartoon pictures illustrating bubble evolution and black hole formation in the limit of very large ρ_b . (a) After inflation, the bubble runs into the fluid with a large Lorentz factor. (b) fluid freely flows inside as the bubble expands into the homogeneous background. Due to the large ρ_b , fluid that flows in soon gets diluted. (c) As the radiation density outside the bubble decreases due to Hubble expansion, fluid that flows into the growing bubble becomes insignificant, and the bubble mass is dominated by the interior vacuum and the bubble wall. For an exterior observer, the bubble begins to turn around at t_s . (d) After t_s , the physical size of the bubble continues to grow and then exceeds the de Sitter horizon associated with the interior vacuum. The bubble would then inflate into a baby universe, which is connected to us by a wormhole. The wormhole would eventually pinch off, turning into a black hole. The white region around the wormhole throat represents an almost empty shell, where the fluid gets significantly diluted by the bubble's interior vacuum before t_s . For an exterior FRW observer, there is a spherical rarefaction wave propagating outwards.

limits. During inflation, bubbles grow exponentially and their sizes spread over a large range of scales, therefore the resulting black holes should have an extended mass spectrum. Now we would like to compute this spectrum.

Bubbles formed earlier expand to larger sizes, but their number density gets more diluted

by the cosmic expansion. By assuming that the bubbles are formed with a vanishing size and that the bubble worldsheet can be approximated by the future light cone of the nucleation point, one can find that the number density of bubbles having radius in the interval $(\chi_i, \chi_i + d\chi_i)$ at t ($t > t_i$) is [41]

$$dn(t) \approx \lambda \frac{d\chi_i}{a(t)^3 (\chi_i + H_i^{-1})^4}. \quad (22)$$

where λ is the bubble nucleation rate per Hubble spacetime volume H_i^{-4} .

It is convenient to use the standard mass function to characterize the spectrum of PBHs,

$$f(M) = \frac{M^2}{\rho_{CDM}(t)} \frac{dn(t)}{dM}, \quad (23)$$

where ρ_{CDM} is the mass density of cold dark matter. This can be interpreted as the fraction of dark matter in PBHs at M within the mass range $\Delta M \sim M$. Because the black hole density and dark matter density are diluted by the cosmic expansion in the same way, $f(M)$ is a constant over time. The total fraction of dark matter in PBHs can be obtained by integrating the mass function, and is given by

$$f_{PBH} = \int \frac{dM}{M} f(M), \quad (24)$$

which should satisfy $f_{PBH} \leq 1$. During the radiation era,

$$\rho_{CDM}(t) \sim \frac{M_{Pl}^3}{Bt^{3/2} \mathcal{M}_{eq}^{1/2}}, \quad (25)$$

where $B \sim 10$ is a constant and $\mathcal{M}_{eq} \sim 10^{17} M_\odot$ is the dark matter mass within a Hubble radius at dust-radiation equality. Then the mass function can be written as

$$f(M) \sim \frac{B\lambda \mathcal{M}_{eq}^{1/2}}{M_{Pl}^3} \frac{M^2}{H_i^{3/2} (\chi_i + H_i^{-1})^4} \frac{d\chi_i}{dM}. \quad (26)$$

In the following we will only show results in the limit of negligible ρ_b , because we found that mass spectra in this limit have the most interesting features in our model. In order to find $f(M)$, we need the relation between M and χ_i . This can be obtained by numerically solving eq. (7) and using eq. (13). The mass function is completely determined by the following five quantities: the Lorentz factor of the bubble wall γ_i at the end of inflation, the bubble wall tension σ , the interior vacuum density ρ_b , the inflationary density ρ_i , and the bubble nucleation rate λ . It would be more convenient to specify the mass function with

parameters $\gamma_i, \lambda, M_* \equiv H_\sigma^{-1}$ and $\eta_i \equiv H_i^{1/2}$, where η_i characterizes the inflationary energy scale. The specific value of ρ_b is not important as long as we have $H_b \ll H_\sigma$.

Several curves of $f(M)$ are shown in fig. 4. Depending on the parameters, the mass function can have very different shapes and can be either wide or relatively narrow. Specifically, in fig. 4 we fix all other parameters except for the Lorentz factor γ_i . For small γ_i , the maximum of $f(M)$ appears at M_* , and $f(M) \propto M^{1/4}$ near M_* in the subcritical regime. This is consistent with the results in refs. [39, 40]. As γ_i increases, another peak develops at M_{min} (which is the black hole mass from a bubble with $\chi_i = H_i^{-1}$), and the spectrum becomes gradually spiky, with the black hole population dominated by those with mass $\sim M_{min}$. When γ_i is sufficiently large, all bubble are in the supercritical regime. We can also see that for large masses, all spectra converge to the same straight line. It is shown in the appendix that for very large bubbles ($\chi_i \gg H_i^{-1}$), a_s is a constant independent of χ_i (eq. (49)). For supercritical bubbles, we have $M \sim H_i \chi_s^2 \sim H_i (\chi_i + a_s H_i^{-1})^2$, then by eq. (26) we have

$$f(M) \propto \frac{M^{-1/2}}{\left[1 - a_s (H_i M)^{-1/2}\right]^4}. \quad (27)$$

For $M \rightarrow \infty$, this gives $f(M) \propto M^{-1/2}$, which explains the converging behavior of the mass functions for large masses. We also note that the values of $f(M_{min})$ in different spectra (of varying γ_i) seem to be on a straight line in fig. 4, which suggests a power function $f(M_{min}) \propto M_{min}^\alpha$. Since the explicit relation between M and χ_i (hence the relation between $f(M)$ and M) is unknown, the power α cannot be determined analytically. Numerically we found $\alpha \approx 1$.

V. OBSERVATIONAL BOUNDS

The mass function of a certain PBH model is constrained by observations: based on dynamical, microlensing and astrophysical effects, different observational missions have placed (stringent) upper bounds on the population of PBHs in different mass ranges. Some conservative and up-to-date constraints are shown in fig. 1 on the total fraction of dark matter in PBHs at $\sim 10^{15}$ – 10^{47} g. The colored regions have been excluded by observations. These bounds are valid only for monochromatic PBHs, i.e., PBHs of almost the same mass with a narrow spectrum. We can see that the only window allowing PBHs to constitute all dark

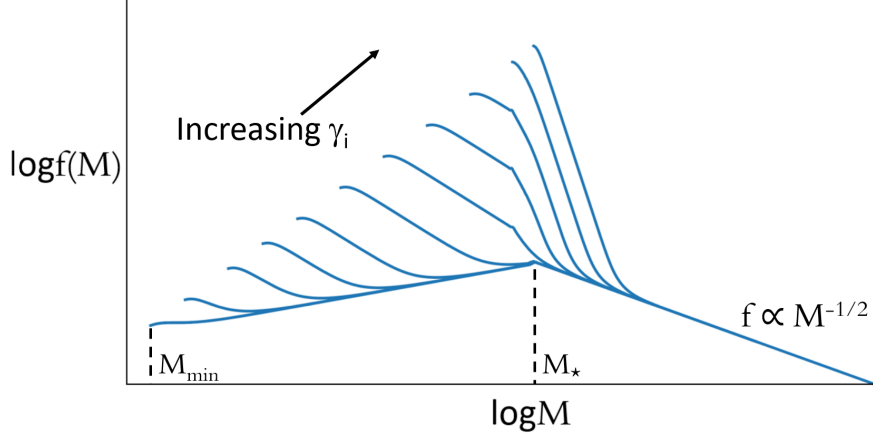


FIG. 4: Some examples of the mass function $f(M)$ in the limit of negligible ρ_b , covering masses above M_{min} . We have fixed parameters except for the Lorentz factor γ_i . For small γ_i the maximum of $f(M)$ appears at M_* . As γ_i increases, another peak develops at M_{min} . For large γ_i , $f(M_{min})$ becomes larger than $f(M_*)$, and the spectrum turns spiky. For large masses, all spectra approach to $f \propto M^{-1/2}$.

matter is at $\sim 10^{17}$ – 10^{23} g. If we would like to explain LIGO/Virgo events with PBHs, there should be a sufficient number of them around $\sim 10M_\odot$. Likewise, if SMBHs were seeded by PBHs, there should be enough of them at $M \gtrsim 10^3 M_\odot$ such that the number density of the seeds exceeds that of galaxies observed today. With an increasing number of observations and studies imposing more and more bounds, it seems difficult for PBHs to completely account for all three of them, unless the mass spectrum has multiple spikes [45, 46].

For an extended mass spectrum, such as the one given by eq. (26), fig. 1 cannot be adopted directly. But one can apply the method developed in ref. [47], using the bounds in fig. 1 to constrain the parameters in the extended spectrum. Ref. [47] shows that the mass function $f(M)$ should satisfy the following condition,

$$\sum_j \left(\int_{M_{j_1}}^{M_{j_2}} \frac{dM}{M} \frac{f(M)}{f_{j,max}(M)} \right)^2 < 1, \quad (28)$$

where j denotes different observations, with (M_{j_1}, M_{j_2}) the mass range covered by that particular observation, and $f_{j,max}(M)$ the corresponding upper bound. Loosely speaking, however, as long as $f(M)/M$ does not have a plateau over a relatively big range, we can constrain a certain model by placing $f(M)$ in fig. 1 while avoiding hitting the excluded regions. For this reason, we show $f(M)$ and $f_{max}(M)$ in the same figure (fig. 5), even

though they represent different quantities.

Fig. 5 shows four interesting examples of our mass function in the limit of negligible ρ_b . Firstly, the blue (solid) curve and the orange (dashed) curve are two examples consistent with PBHs being all dark matter as well as the seeds for SMBHs. The blue one is produced by setting $\gamma_i = 10^3$, $M_* = 10^{20}$ g, $\lambda \approx 10^{-17}$ and $\eta_i \approx 10^8$ GeV, and covers the mass range beyond $\sim 10^{17}$ g; the orange one is from $\gamma_i = 10^{23}$, $M_* = 10^{20}$ g, $\lambda \approx 10^{-9}$ and $\eta_i \approx 10^5$ GeV, and covers the mass range beyond $\sim 10^{18}$ g. Both curves have their maximum value $f = \mathcal{O}(0.1-1)$ on the lower end, where $f_{max}(M)$ is poorly constrained. As a result, PBHs with these spectra can account for all dark matter ($f_{PBH} = 1$). In addition, these two spectra may also provide the seeds for SMBHs. At the present time (t_0), the number density of PBHs of mass $\sim M$ is approximately given by

$$n(M) \sim \rho_{CDM}(t_0) \frac{f(M)}{M} \approx 4 \times 10^{11} \left(\frac{M_\odot}{M} \right) f(M) \text{ Mpc}^{-3}. \quad (29)$$

It was shown in ref. [9] that PBHs at $z \sim 6$ with masses $10^2 M_\odot \lesssim M \lesssim 10^4 M_\odot$ can attain sufficient accretion, growing to SMBHs at the present time, even if $f(M)$ is as small as 10^{-9} in that mass range. Therefore, in order to serve as seeds for SMBHs, PBHs should have masses $M \gtrsim 10^2 M_\odot$. We can see from the two curves that $f(10^3 M_\odot) \sim 10^{-9}$, which gives $n(10^3 M_\odot) \sim 0.4 \text{ Mpc}^{-3}$. This is larger than the galaxy density $n_G \sim 0.1 \text{ Mpc}^{-3}$. Therefore it is possible that SMBHs observed today were seeded by these PBHs.

The green (dashdotted) curve in fig. 5 is produced by setting $\gamma_i = 10^{11}$, $M_* = M_\odot$, $\lambda \approx 10^{-12}$ and $\eta_i \approx 10^6$ GeV. It covers the mass range $\sim 10^{18}-10^{35}$ g. PBHs with this spectrum can also account for all dark matter. As the mass increases, $f(M)$ reaches a minimum at $\sim 10^{26}$ g and increases to $f \sim 0.01$ around the transition mass $M_* = M_\odot$. In order to reproduce the black hole merger rate inferred by the LIGO/Virgo events, the mass function should have $f(M \sim 10 M_\odot) = \mathcal{O}(10^{-3}-10^{-2})$ [4, 8, 48, 49]. Therefore, our model is able to provide a primordial explanation to those detections. However, note that in order not to hit the bound imposed by black hole accretion [9] (the pink region in fig. 1), there should be a cutoff at around $200 M_\odot$. Physically, such a cutoff can be achieved if we relax the assumption that bubbles nucleate with a constant rate during inflation. This is possible especially in inflationary models where the inflaton travels for a relatively large distance during the slow-roll.

Lastly, the red (dotted) curve in fig. 5 is $f(M)$ with $\gamma_i = 10^{18}$, $M_* = 10 M_\odot$, $\lambda = 10^{-19}$ and

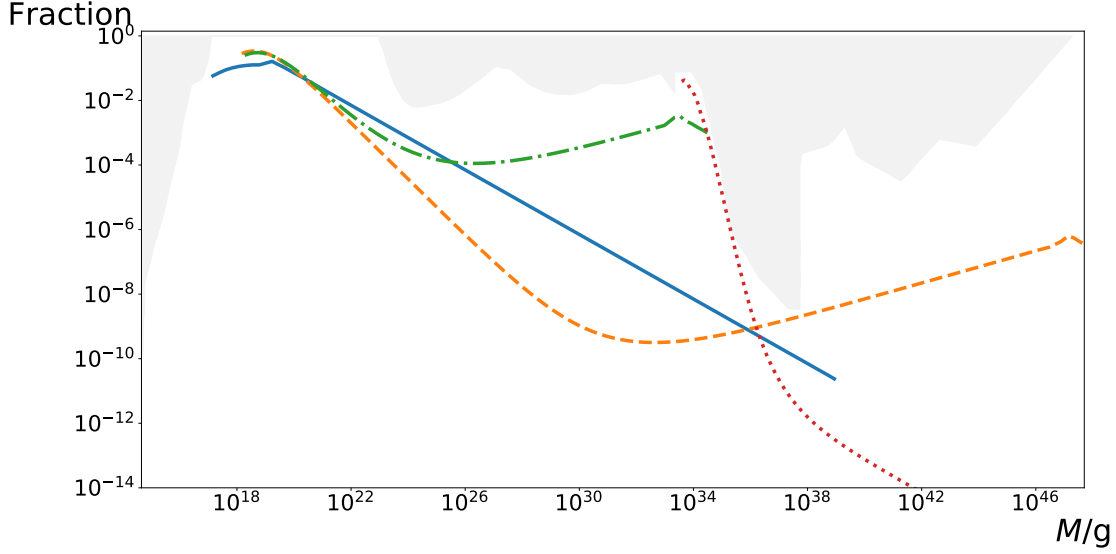


FIG. 5: The light grey shaded areas are observationally excluded regions (also shown in fig. 1). Their bottom boundary is $f_{max}(M)$, the upper bound of the fraction of dark matter in PBHs for a monochromatic mass distribution. The colored curves are four examples of $f(M)$ in the limit of negligible ρ_b , where $f(M)$ can be interpreted as the fraction of dark matter in PBHs within the mass range $M-2M$ for an extended mass distribution. $f_{max}(M)$ and $f(M)$ represent different quantities but we place them in the same figure because $f(M)$ can loosely be constrained by $f_{max}(M)$. The mass range $10^{17}-10^{23}$ g is poorly constrained by observations at the moment, so $f(M) = \mathcal{O}(0.1-1)$ in this window could provide an explanation to all dark matter. The blue (solid) and orange (dashed) curves are two spectra where the PBHs can account for all dark matter and seeds for SMBHs; the green (dashdotted) curve can explain both dark matter and LIGO/Virgo black holes; the red (dotted) curve can explain LIGO/Virgo black holes and SMBHs.

$\eta_i \approx 1$ TeV. It covers the mass range above M_\odot . With this spectrum, we have $f(10M_\odot) = \mathcal{O}(10^{-3}-10^{-2})$, hence these PBHs can account for the LIGO/Virgo black holes. In addition, we can see that $f(10^3M_\odot) \sim 10^{-9}$, so these PBHs could also be the seeds of SMBHs. The maximum of mass function is at $M_{min} \sim M_\odot$, where $f = \mathcal{O}(0.01-0.1)$, so these black holes can constitute no more than 10% of the dark matter. Another noticeable feature of this spectrum is that it corresponds to an inflationary energy scale $\eta_i \sim 1$ TeV, which is the smallest one can envision for inflation.

VI. SUMMARY AND DISCUSSION

In this paper we have studied a mechanism of primordial black hole formation, where the black holes are formed by vacuum bubbles that randomly nucleate during inflation. This is a natural outcome if the inflaton runs in a general, multi-dimensional potential, where there could be many vacua and thus many tunneling channels. Typically, these bubbles expand with an acceleration and soon acquire a large Lorentz factor. Inflaton outside the bubbles thermalize into radiation fluid at the end of inflation, which is then run into by the fast expanding bubbles. If there are no couplings between the bubble fields and the standard model particles other than gravity, the fluid would then freely flow in as the bubbles grow possibly by many orders of magnitude. In the meantime the interior vacuum and the wall tension tend to slow down the bubble expansion. The bubble wall's trajectory can be found by matching the spacetimes on two sides of the wall without the knowledge of the fluid's motion, since the exterior spacetime can be described by a flat FRW metric. This works till the time when the bubble comes to a halt with respect to the Hubble flow (at a comoving radius denoted by χ_s), because after that the bubble turns around and interacts with the interior inhomogeneous fluid, and neither side of the wall can now be expressed in a closed form. Therefore, in order to accurately describe the evolution of the bubbles as well as the radiation fluid, one needs to turn to numerical study. This may be challenging because one has to deal with a thin wall with a large Lorentz factor traveling a long distance.

However, if we focus on the case of a small bubble wall tension, and consider the extreme limits of small and large interior vacuum density ρ_b , the fate of the bubble can easily be estimated. In the limit of very small ρ_b , where ρ_b is assumed to be at all times subdominant compared to the radiation density, the bubble can be regarded as a spherical domain wall moving in homogeneous fluid, since the bubble grows at a speed close to that of light for most of the time before it comes to a stop. In the limit of very large ρ_b , the fluid that flows in soon gets diluted and could eventually be neglected compared to the interior vacuum, hence the bubble can be regarded as a pure vacuum bubble. Black holes would form in both scenario, either in the subcritical or in the supercritical regime, and we found estimates for the resulting black hole masses.

For completeness, we shall now (qualitatively) comment on a situation not captured in our previous analysis (subsection III A). In the limit of negligible ρ_b , the estimate of the

black hole mass from subcritical bubbles is directly related to R_{max} , the maximum value of the bubble's physical radius, which can be approximated by the cosmic horizon at the Hubble crossing of a test wall at χ_s . However, by doing this we have assumed that the interior spacetime near the bubble wall can be approximated by an FRW metric dominated by radiation (see fig. 2), but this is no longer true if the bubble comes within the spherical rarefaction wave before Hubble crossing, which would happen to bubbles with $\chi_s \sim \chi_i$, as we found in subsection III A. This can be avoided if $a_s \sim H_i (\chi_s - \chi_i)$ is sufficiently large for all subcritical bubbles, but if it did happen to some bubbles, possibly close to the transition regime, they may either (i) become supercritical because the region inside the rarefaction wave front has a lower radiation density, thus a smaller cosmic expansion rate, which may be smaller than the expansion rate H_σ on the bubble wall; or (ii) acquire a $R_{max} < R_H$ due to the smaller cosmic expansion rate inside the wave front, in which case the estimate $M \sim 4\pi\sigma R_H^2$ becomes an upper bound. In either case, we expect that this would simply smooth the mass function near the transition regime, instead of bringing a spike.

Our main results are in fig. 5, where we show several examples of the mass spectrum of the black holes in the limit of very small ρ_b . Depending on the model parameters, the mass distribution of these black holes could either be extended or spiky, and may have two peaks separated by a wide mass range. Constrained by the current observational bounds, our model is able to simultaneously explain the origin of any two of the following three puzzles: dark matter, black holes detected by LIGO/Virgo ($M = \mathcal{O}(10\text{--}100)M_\odot$), and supermassive black holes at the center of most galaxies ($M = \mathcal{O}(10^6\text{--}10^{10})M_\odot$). Of course, one could envisage that there exist multiple tunneling channels during inflation, which allow the formation of bubbles with different properties. Then it is possible that the resulting black holes have a spectrum with more than two peaks.

Finally, we note that all astrophysically interesting spectra in our model require a small energy scale of inflation, the largest one being 10^8 GeV, and the smallest one 1 TeV, which is the lowest one would expect for an inflationary model (although the definite bound is at the MeV scale, consistent with Big Bang Nucleosynthesis). A lower bound on the inflationary scale possibly determined in the future may thus impose a serious constraint on our model.

Appendix: Spacetime matching on bubble wall

In this appendix we study the dynamics of the bubble by matching the spacetimes on two sides of the wall according to the Israel junction conditions [50, 51]. The bubble wall's equation of motion will be derived, as well as the bubble mass during the collapse. We closely follow the method and notations in ref. [52]

After inflation, the bubble runs into the ambient radiation fluid at a speed close to that of light. Since we assume there is only gravitational interaction between the bubble and the fluid, the fluid freely flows in, and the exterior spacetime can be described by a flat FRW metric,

$$ds^2 = dt^2 - a^2(t)(dr^2 + r^2 d\Omega^2). \quad (30)$$

The metric of the bubble interior can be expressed as

$$ds^2 = dt^2 - a_1(r, t)^2 dr^2 - a_2(r, t)^2 r^2 d\Omega^2. \quad (31)$$

For a thin wall, we can use the Israel junction conditions to match these two metrics.

Let the trajectory of the wall be $(t(\tau), \chi(\tau))$, where τ is the proper time on the wall. Then a vector tangent to the wall is $v^\mu = (t_{,\tau}, \chi_{,\tau})$, where $_{,\tau} \equiv d/d\tau$. Assuming \dot{t} to be positive and $v^\mu v_\mu = -1$, we have $t_{,\tau} = \sqrt{1 + a_1^2 \chi_{,\tau}^2}$. Let ξ^μ be the normal unit vector on the wall. Then $\xi^\mu v_\mu = 0$ and $\xi^\mu \xi_\mu = 1$ give $\xi^\mu = (a_1 \chi_{,\tau}, t_{,\tau}/a_1)$ and $\xi_\mu = (-a_1 \chi_{,\tau}, a_1 t_{,\tau})$. We also define the notations $[Q] \equiv Q_{out} - Q_{in}$, $\{Q\} \equiv Q_{out} + Q_{in}$, and $\bar{Q} \equiv (Q_{out} + Q_{in})/2$, where “out” and “in” denote matching quantities on different sides of the hypersurface.

The induced metric on the wall is defined to be $h_{\mu\nu} = g_{\mu\nu} - \xi_\mu \xi_\nu$. Then the first junction condition is $[h_{\mu\nu}] = 0$. The (t, t) and (θ, θ) components give

$$a_1^2 = a_2^2 = a^2. \quad (32)$$

Therefore $a_{1,\tau} = a_{2,\tau} = a_{,\tau}$, which gives

$$\dot{a} t_{,\tau} = a_{,\tau} = t_{,\tau} \dot{a}_1 + r_{,\tau} a_1' = t_{,\tau} \dot{a}_2 + r_{,\tau} a_2', \quad (33)$$

where the overdot and the prime stand for the first derivative with respect to t and r , respectively.

The extrinsic curvature of the wall is $K_{\mu\nu} = h_\mu^\alpha \nabla_\alpha \xi_\nu$, where ∇ is the covariant derivative operator for 4-spacetime. Then the second junction condition is $[K_{\mu\nu}] = 8\pi(-S_{\mu\nu} + S h_{\mu\nu}/2)$,

where $S_{\mu\nu} = -\sigma h_{\mu\nu}$ is the energy-momentum tensor of the domain wall, σ being the surface energy. The (θ, θ) component then gives

$$[\xi^\mu \partial_\mu \ln(a_2 \chi)] = -4\pi\sigma. \quad (34)$$

Right inside and outside the bubble wall, we have

$$\xi^\mu \partial_\mu \ln(a_2 \chi)|_{in} = a_1 \chi_{,\tau} \frac{\dot{a}_2}{a_2} + \frac{t_{,\tau}}{a_1} \left(\frac{a'_2}{a_2} + \frac{1}{\chi} \right), \quad (35)$$

$$\xi^\mu \partial_\mu \ln(a \chi)|_{out} = r_{,\tau} \dot{a} + \frac{t_{,\tau}}{a \chi}, \quad (36)$$

respectively. Then eq. (34) yields

$$a'_2 = 4\pi\sigma a^2 \sqrt{1 + (a \chi_{,\tau})^2}. \quad (37)$$

The (τ, τ) component of the second junction condition gives

$$[\xi_\mu D_\tau v^\mu] = -4\pi\sigma, \quad (38)$$

where $D_\tau v^\mu = \partial_\tau v^\mu + \Gamma_{\lambda\sigma}^\mu v^\lambda v^\sigma$, with $\Gamma_{\lambda\sigma}^\mu$ the Christoffel symbols in 4-spacetime. Right inside and outside the bubble wall, we have

$$\xi_\mu D_\tau v^\mu|_{in} = \frac{(a_1 \chi_{,\tau})_{,\tau}}{t_{,\tau}} + \dot{a}_1 \chi_{,\tau}, \quad (39)$$

$$\xi_\mu D_\tau v^\mu|_{out} = \frac{a \chi_{,\tau\tau} + 2a_{1,\tau} \chi_{,\tau}}{t_{,\tau}}, \quad (40)$$

respectively. Hence eq. (38) gives

$$a'_1 = -\frac{4\pi\sigma \sqrt{1 + (a \chi_{,\tau})^2}}{\chi_{,\tau}^2}. \quad (41)$$

Converting τ to t , a'_1 and a'_2 can be rewritten as

$$a'_1 = -\frac{4\pi\sigma \sqrt{1 - (a \dot{\chi})^2}}{\dot{\chi}^2}, \quad (42)$$

$$a'_2 = \frac{4\pi\sigma a^2}{\sqrt{1 - (a \dot{\chi})^2}}. \quad (43)$$

The equation of motion for the wall is given by $S_{\mu\nu} \bar{K}^{\mu\nu} = [T_{\mu\nu} \xi^\mu \xi^\nu]$. A perfect fluid has energy-momentum tensor $T_{\mu\nu} = (\rho + p)u_\mu u_\nu + p g_{\mu\nu}$. Note that the interior vacuum pressure $p_b = -\rho_b$, while the radiation pressure $p_r = \rho_r/3$. Then we have

$$\{\xi_\mu D_\tau v^\mu + 2\xi^\mu \partial_\mu \ln(a_2 \chi)\} = -\frac{2}{\sigma} [(\rho + p)(u^\mu \xi_\mu)^2 + p]. \quad (44)$$

Now we assume $[u_\mu \xi^\mu] = 0$, and $[\rho_r] = 0$. Since $u_\mu \xi^\mu$ is the 4-velocity of the fluid in the direction of the unit normal vector, these two conditions mean the radiation fluid flows through the wall smoothly. Then the equation of motion (eq. (44)) yields

$$\ddot{\chi} + (4 - 3a^2 \dot{\chi}^2) H \dot{\chi} + \frac{2}{a^2 \chi} (1 - a^2 \dot{\chi}^2) = - \left(\frac{\rho_b}{\sigma} + 6\pi\sigma \right) \frac{(1 - a^2 \dot{\chi}^2)^{3/2}}{a}, \quad (45)$$

where $H \equiv \dot{a}/a = (2t)^{-1}$ is the Hubble parameter. Let t_i be the time when inflation ends, and the scale factor $a = (t/t_i)^{1/2}$. The bubble expands with initial conditions $\chi(t_i) = \chi_i$ and $\dot{\chi}(t_i) = (1 - \gamma_i^{-2})^{1/2}$, where γ_i is the Lorentz factor of the bubble wall at t_i . Since γ_i is assumed to be large, the trajectory of the wall can be approximated by $a\dot{\chi} \approx 1$ (at least at early times), where the overdot represents the first derivative with respect to t . This gives

$$\chi(t) \approx \chi_i + 2\sqrt{t_i}(\sqrt{t} - \sqrt{t_i}), \quad (46)$$

For a bubble far beyond the Hubble horizon at t_i , the trajectory of the wall can be obtained analytically. For an exterior FRW observer, the Lorentz factor of the wall is $\gamma(t) = (1 - a^2 \dot{\chi}^2)^{-1/2}$. Define $u \equiv \sqrt{\gamma^2 - 1}$, then eq. (45) can be rewritten as

$$\dot{u} + \frac{3}{2t}u + \frac{2\gamma}{a\chi} + \frac{\rho_b}{\sigma} + 6\pi\sigma = 0. \quad (47)$$

By eq. (46), the physical radius of the wall is $a\chi \approx a(\chi_i - H_i^{-1}) + 2t$. If χ_i is sufficiently large ($\chi_i \gg H_i^{-1}$), the third term in eq. (47) can be neglected compared to the second one. Then u has an analytic solution

$$u(t) \approx \left[\gamma_i t_i^{3/2} + \frac{2}{5} \left(\frac{\rho_b}{\sigma} + 6\pi\sigma \right) (t_i^{5/2} - t^{5/2}) \right] t^{-3/2}. \quad (48)$$

Let t_s be the time when the bubble wall comes to a stop with respect to the Hubble flow. We have $\gamma(t_s) = 1$, or $u(t_s) = 0$. Then eq. (48) gives

$$a_s \equiv a(t_s) = \left[\frac{5\gamma_i}{2t_i} \left(\frac{\rho_b}{\sigma} + 6\pi\sigma \right)^{-1} + 1 \right]^{1/5}. \quad (49)$$

Note that to obtain this result we have assumed $\chi_i \gg H_i^{-1}$. Due to the third term in eq. (47), which tends to slow down the bubble, the actual a_s could be significantly smaller. For more general cases we need to numerically solve eq. (45) or eq. (47) in order to find out the bubble wall's trajectory before t_s .

After t_s , the bubble turns around for an FRW observer, and runs into the interior fluid. In some situations (see main text) the interior can be approximately described by an FRW

universe dominated by radiation (ρ_r) and a vacuum (ρ_b). In this case we can still use junction conditions to match the interior and exterior regions, then eqs. (42), (43) and (45) become

$$a'_1 = \frac{4\pi\sigma\sqrt{1-a^2\dot{\chi}^2}}{\dot{\chi}^2}, \quad (50)$$

$$a'_2 = -\frac{4\pi\sigma a^2}{\sqrt{1-a^2\dot{\chi}^2}}, \quad (51)$$

$$\ddot{\chi} + (4 - 3a^2\dot{\chi}^2) H\dot{\chi} + \frac{2}{a^2\chi} (1 - a^2\dot{\chi}^2) = -\left(\frac{\rho_b}{\sigma} - 6\pi\sigma\right) \frac{(1 - a^2\dot{\chi}^2)^{3/2}}{a}. \quad (52)$$

Here a becomes the scale factor inside the bubble, and a_1, a_2 become the metric functions outside. a and H are now determined by the Friedmann equations,

$$H^2 = \frac{8\pi}{3} (\rho_b + \rho_r^{(in)}), \quad (53)$$

$$\frac{\ddot{a}}{a} = \frac{8\pi}{3} (\rho_b - \rho_r^{(in)}), \quad (54)$$

where $\rho_r^{(in)}(t)$ is the interior radiation density near the bubble wall.

Furthermore, we can use eq. (50) and (51) to find the mass measured right outside the bubble. Here we use the standard Misner-Sharp quasi-local mass to characterize the total mass enclosed by a sphere [53, 54]. In our coordinates, the Misner-Sharp mass right outside the wall is

$$M = \frac{a_2\chi}{2} \left(1 - \frac{(a_2\chi)'^2}{a_1^2} + (a_2\dot{\chi})^2 \right) \quad (55)$$

$$= \frac{1}{2} H^2 (a\chi)^3 + \frac{4\pi\sigma (a\chi)^2}{\sqrt{1-(a\dot{\chi})^2}} + \frac{4\pi\sigma H\dot{\chi}}{\chi\sqrt{1-(a\dot{\chi})^2}} (a\chi)^4 - 8\pi^2\sigma^2 (a\chi)^3 \quad (56)$$

$$= \frac{4}{3}\pi (\rho_r + \rho_b) R^3 + 4\pi\sigma\gamma R^2 + 4\pi\sigma H\sqrt{\gamma^2 - 1} R^3 - 8\pi^2\sigma^2 R^3, \quad (57)$$

where $R = a\chi$ is the physical radius of the bubble and γ is the bubble wall's Lorentz factor for an interior FRW observer. Here the four terms are the volume energy, surface energy, surface-volume binding energy and surface-surface binding energy, respectively. The black hole mass can be determined by reading the value of M when the bubble's radius decreases to the Schwarzschild radius, i.e., $R = 2M$. The black hole mass obtained in this way is more precise than eq. (19), but we have verified that the difference can be neglected when computing the mass spectrum of the black holes.

Acknowledgments

I would like to thank Alex Vilenkin for stimulating discussion and comments. This work is supported by the U.S. Department of Energy, Office of High Energy Physics, under Award No. DE-SC0019470 at Arizona State University.

-
- [1] B. Abbott et al. (LIGO Scientific, Virgo), *Phys. Rev. X* **9**, 031040 (2019), 1811.12907.
 - [2] S. Bird, I. Cholis, J. B. Muñoz, Y. Ali-Haïmoud, M. Kamionkowski, E. D. Kovetz, A. Racanelli, and A. G. Riess, *Phys. Rev. Lett.* **116**, 201301 (2016), 1603.00464.
 - [3] S. Clesse and J. García-Bellido, *Phys. Dark Univ.* **15**, 142 (2017), 1603.05234.
 - [4] M. Sasaki, T. Suyama, T. Tanaka, and S. Yokoyama, *Phys. Rev. Lett.* **117**, 061101 (2016), 1603.08338.
 - [5] B. Carr and F. Kuhnel (2020), 2006.02838.
 - [6] M. Sasaki, T. Suyama, T. Tanaka, and S. Yokoyama, *Class. Quant. Grav.* **35**, 063001 (2018), 1801.05235.
 - [7] B. Carr, K. Kohri, Y. Sendouda, and J. Yokoyama (2020), 2002.12778.
 - [8] V. Vaskonen and H. Veermäe, *Phys. Rev. D* **101**, 043015 (2020), 1908.09752.
 - [9] P. D. Serpico, V. Poulin, D. Inman, and K. Kohri (2020), 2002.10771.
 - [10] D. Lynden-Bell, *Nature* **223**, 690 (1969).
 - [11] J. Kormendy and D. Richstone, *Ann. Rev. Astron. Astrophys.* **33**, 581 (1995).
 - [12] Z. Haiman, *Astrophys. J.* **613**, 36 (2004), astro-ph/0404196.
 - [13] J. Kormendy and L. C. Ho, *Ann. Rev. Astron. Astrophys.* **51**, 511 (2013), 1304.7762.
 - [14] S. G. Rubin, A. S. Sakharov, and M. Yu. Khlopov, *J. Exp. Theor. Phys.* **91**, 921 (2001), [*J. Exp. Theor. Phys.* 92,921(2001)], hep-ph/0106187.
 - [15] R. Bean and J. Magueijo, *Phys. Rev.* **D66**, 063505 (2002), astro-ph/0204486.
 - [16] N. Duechting, *Phys. Rev.* **D70**, 064015 (2004), astro-ph/0406260.
 - [17] S. Clesse and J. García-Bellido, *Phys. Rev.* **D92**, 023524 (2015), 1501.07565.
 - [18] B. Carr and J. Silk, *Mon. Not. Roy. Astron. Soc.* **478**, 3756 (2018), 1801.00672.
 - [19] P. Ivanov, P. Naselsky, and I. Novikov, *Phys. Rev.* **D50**, 7173 (1994).
 - [20] J. Garcia-Bellido, A. D. Linde, and D. Wands, *Phys. Rev.* **D54**, 6040 (1996), astro-

ph/9605094.

- [21] M. Kawasaki, N. Sugiyama, and T. Yanagida, Phys. Rev. **D57**, 6050 (1998), hep-ph/9710259.
- [22] J. Yokoyama, Phys. Rev. **D58**, 083510 (1998), astro-ph/9802357.
- [23] J. Garcia-Bellido and E. Ruiz Morales, Phys. Dark Univ. **18**, 47 (2017), 1702.03901.
- [24] M. P. Hertzberg and M. Yamada, Phys. Rev. **D97**, 083509 (2018), 1712.09750.
- [25] J. Chluba, R. Khatri, and R. A. Sunyaev, Mon. Not. Roy. Astron. Soc. **425**, 1129 (2012), 1202.0057.
- [26] J. Chluba, A. L. Erickcek, and I. Ben-Dayan, Astrophys. J. **758**, 76 (2012), 1203.2681.
- [27] K. Kohri, T. Nakama, and T. Suyama, Phys. Rev. **D90**, 083514 (2014), 1405.5999.
- [28] T. Nakama, B. Carr, and J. Silk, Phys. Rev. **D97**, 043525 (2018), 1710.06945.
- [29] T. Nakama, T. Suyama, and J. Yokoyama, Phys. Rev. **D94**, 103522 (2016), 1609.02245.
- [30] S. W. Hawking, Phys. Lett. **B231**, 237 (1989).
- [31] A. Polnarev and R. Zembowicz, Phys. Rev. **D43**, 1106 (1991).
- [32] J. Garriga and A. Vilenkin, Phys. Rev. **D47**, 3265 (1993), hep-ph/9208212.
- [33] R. R. Caldwell and P. Casper, Phys. Rev. **D53**, 3002 (1996), gr-qc/9509012.
- [34] S. W. Hawking, I. G. Moss, and J. M. Stewart, Phys. Rev. **D26**, 2681 (1982).
- [35] M. Khlopov, R. Konoplich, S. Rubin, and A. Sakharov, Grav. Cosmol. **2**, S1 (1999), hep-ph/9912422.
- [36] I. Dymnikova, L. Koziel, M. Khlopov, and S. Rubin, Grav. Cosmol. **6**, 311 (2000), hep-th/0010120.
- [37] S. G. Rubin, M. Yu. Khlopov, and A. S. Sakharov, Grav. Cosmol. **6**, 51 (2000), hep-ph/0005271.
- [38] M. Yu. Khlopov, S. G. Rubin, and A. S. Sakharov, Astropart. Phys. **23**, 265 (2005), astro-ph/0401532.
- [39] J. Garriga, A. Vilenkin, and J. Zhang, JCAP **1602**, 064 (2016), 1512.01819.
- [40] H. Deng, J. Garriga, and A. Vilenkin, JCAP **1704**, 050 (2017), 1612.03753.
- [41] H. Deng and A. Vilenkin, JCAP **1712**, 044 (2017), 1710.02865.
- [42] V. Berezin, V. Kuzmin, and I. Tkachev, Phys. Rev. D **36**, 2919 (1987).
- [43] A. Vilenkin, Phys. Lett. **133B**, 177 (1983).
- [44] J. Ipser and P. Sikivie, Phys. Rev. **D30**, 712 (1984).
- [45] Y.-F. Cai, X. Tong, D.-G. Wang, and S.-F. Yan, Phys. Rev. Lett. **121**, 081306 (2018),

1805.03639.

- [46] B. Carr and F. Kuhnel, Phys. Rev. D **99**, 103535 (2019), 1811.06532.
- [47] B. Carr, M. Raidal, T. Tenkanen, V. Vaskonen, and H. Veermäe, Phys. Rev. **D96**, 023514 (2017), 1705.05567.
- [48] Y. Ali-Haïmoud, E. D. Kovetz, and M. Kamionkowski, Phys. Rev. D **96**, 123523 (2017), 1709.06576.
- [49] V. De Luca, G. Franciolini, P. Pani, and A. Riotto (2020), 2005.05641.
- [50] W. Israel, Nuovo Cim. B **44S10**, 1 (1966), [Erratum: Nuovo Cim.B 48, 463 (1967)].
- [51] K.-i. Maeda, Gen. Rel. Grav. **18**, 931 (1986).
- [52] N. Tanahashi and C.-M. Yoo, Class. Quant. Grav. **32**, 155003 (2015), 1411.7479.
- [53] C. W. Misner and D. H. Sharp, Phys. Rev. **136**, B571 (1964).
- [54] S. A. Hayward, Phys. Rev. **D53**, 1938 (1996), gr-qc/9408002.